AD-A056 411 HARRY DIAMOND LABS ADELPHI MD F/G 9/2
REAL-TIME AND MEMORY CORRELATION VIA ACOUSTO-OPTIC PROCESSING,(U)
JUN 78 N J BERG, J N LEE, B J UDELSON

UNCLASSIFIED NL

1 OF 1
AD A056 411

END
DATE FILMED
8-78
DDC

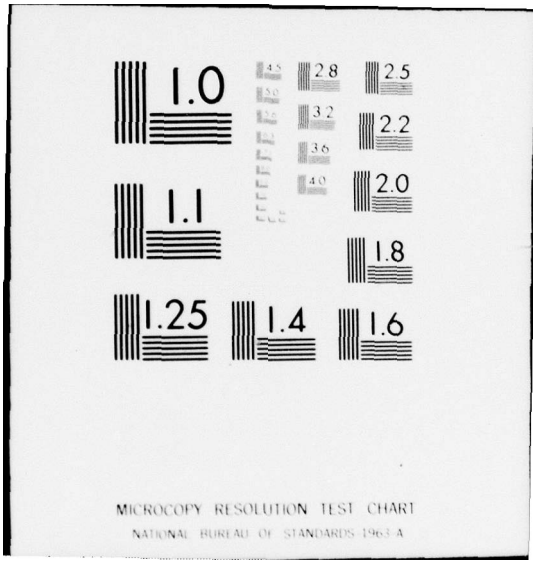
1.0
1.1
1.25
1.4
1.6
1.8
2.0
2.2
2.5
2.8
3.2
3.6
4.0
4.5
5.0
MICROCOPY RESOLUTION TEST CHART
NATIONAL BUREAU OF STANDARDS 1963-A

*BERG, LEE & UDELSON

LEVEL II

REAL-TIME AND MEMORY CORRELATION VIA ACOUSTO-OPTIC PROCESSING

NORMAN J. BERG JOHN N. LEE
BURTON J. UDELSON
US ARMY ELECTRONICS RESEARCH & DEVELOPMENT COMMAND
HARRY DIAMOND LABORATORIES
ADELPHI, MD 20783

Jun 78
13 p.

The requirements of advanced radar systems, secure communications networks, and signal-warfare concepts place severe strains on the capabilities of presently available analog processing technologies. These applications require real-time processing with large bandwidth and dynamic range. The use of acousto-optic technology as an answer to these requirements appears very attractive. Three fundamental signal-processing schemes using the acousto-optic interaction have been investigated: (i) real-time correlation and convolution, (ii) Fourier and discrete Fourier transformation, and (iii) programmable memory correlation. By combining previously known techniques with newly discovered phenomena, major advances in analog signal processing have been demonstrated. Time-bandwidth products in excess of 10,000 and linear dynamic ranges in excess of 50 dB have been achieved with real-time processors. Using the recently discovered acousto-photorefractive effect,[1] storage of surface-acoustic-wave (SAW) signals in lithium niobate ($LiNbO_3$) has been demonstrated. During the information storage time of up to several months, "live" signals can be acousto-optically correlated with the stored signals. This storage phenomenon can be used as the basis for a wide variety of new signal-processing architectures. A description of the experimental results for the real-time processors (correlators and Fourier transformers) and the memory correlator are given in sections II and III, respectively.

II. Real-Time Signal Processing Using Acousto-Optic Interactions

A. Background

The processing of signals using acousto-optic interactions is based on the diffraction of light by refractive index changes induced

163 050

in a piezoelectric material by a surface acoustic wave. Conservation of momentum and energy requires that the frequency of the light diffracted by the propagating surface acoustic wave be shifted by an amount equal to the acoustic frequency.[2] The acousto-optic interaction is normally in the Bragg regime, where the incident light beam is incident at an angle, θ_B, to the SAW front. The sine of θ_B is given by

$$\sin \theta_B = \frac{\lambda_o}{2n\lambda_a} \quad , \tag{1}$$

where λ_o is the wavelength of light in free space, λ_a is the acoustic wavelength in the material, and n is the index of refraction of the material. The Bragg regime permits maximum interaction efficiency, since constructive interference occurs only for the first order diffraction mode, all other modes being suppressed.

For Bragg interaction, the power ratio of diffracted light, I_1, to incident light, I_o is [2]

$$\frac{I_1}{I_o} = \sin^2 \left(1.4\ell\sqrt{M_w P_s}\right) , \tag{2}$$

where M_w is a figure of merit relative to the value for water, ℓ is the interaction length, and P_s is the acoustic power density. For sufficiently small P_s, a linear relationship exists between I_1 and P_s.

The method for achieving convolution via the acousto-optic interaction is indicated in Fig. 1. The amplitude of the light beam that has been diffracted by both acoustic waves, A(t) cos ω_at and B(t) cos ω_at, is proportional to

$$[A(t)\, B(t) \cos (\omega_o - 2\, \omega_a)t] \, , \tag{3}$$

where ω_o is the light frequency. This doubly diffracted beam is collinear with the undiffracted light of intensity I_o, and the two beams are heterodyned in a nonlinear mixer diode. The resultant output voltage is proportional to the product of eq. (3) with cos (ω_ot), and the component at the acoustic frequency ($2\omega_a$) is:

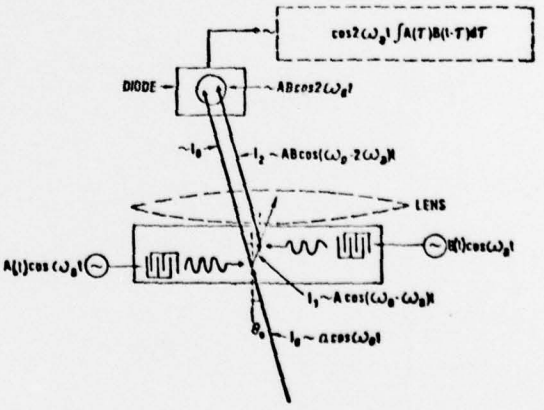

Fig. 1. Waveform Convolution Using Acousto-Optic Bragg Interaction

$$V_{out}(t) \sim A(t)\, B(t) \cos(2\omega_a) \,. \qquad (4)$$

Eq. (4) gives the voltage due to a single light ray. The interaction region between transducers is fully illuminated, and the lens shown in Fig. 1 focuses the entire light beam onto the photo-diode. Recalling that the two signals are physically passing each other, it can be shown that the output voltage as a function of time is given by

$$V_o(t) = \int_{-\infty}^{\infty} A(\tau)B(t - \tau)d\tau \,, \qquad (5)$$

which is equivalent to the convolution of A(t) and B(t).[3] Further, the frequency of the output waveform is twice that of the input waveforms, and the output bandwidth is correspondingly twice the input bandwidth.

One of the primary advantages of using the accusto-optic interaction to obtain convolution (or correlation) as described above is that all nonlinear mixing occurs in the mixer diode. Under these conditions, the piezoelectric material is nondispersive, and the interaction is approximately linear according to Eq. (2). It will also be shown later that large dynamic ranges of signal amplitude are feasible.

The scheme described above uses a single SAW delay line to perform real-time convolution of two rf signals. Correlation is obtained directly if the two signals are symmetric waveforms, since in this case correlation and convolution are equivalent. Correlation of asymmetric waveforms in this scheme may be obtained by time inverting one of the rf inputs. However, the time-inversion process involves additional electronic complexity and problems of the quality of operational performance. As an alternative approach, a "two-crystal" correlator has been designed that uses two separate acoustic delay lines, one of bismuth germanium oxide (BGO) and the other of $LiNbO_3$, placed side by side, as shown in Fig. 2. The incident light passes through the interaction regions of both lines. Since the acoustic wave velocity in BGO is slower (by about half) than the velocity in $LiNbO_3$, an rf signal introduced into $LiNbO_3$ overtakes an rf signal that had been just previously introduced in the BGO. Both the BGO and the $LiNbO_3$ signals are launched in the same direction, thereby obviating time inverting one signal. If the $LiNbO_3$ signal entirely passes the BGO signal, the output at the photodetector corresponds to the correlation of the two waveforms. The maximum pulsewidth that can be completely correlated is equal to one third of the interaction time (or length) of the $LiNbO_3$ delay line. It is important to note that the two signals being correlated acousto-optically are in the form of surface acoustic waves in the $LiNbO_3$ and BGO. To obtain maximum correlation of two propagating signals, their wavelengths and spatial

extent must be the same in both crystals. To accomplish this, the input signal frequencies must be adjusted to be proportional to the ratio of the two SAW velocities, and the input pulse widths must be inversely proportional to this ratio. The correct pulsewidth ratios may be obtained by an auxiliary processing step using the same two-crystal acousto-optic setup.[3]

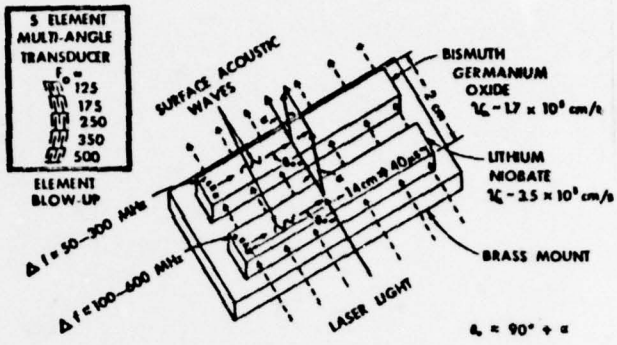

Fig. 2. "Two-Crystal" Waveform Correlation by Using Acousto-Optic Interaction in Adjacent BGO and $LiNbO_3$ Delay Lines.

B. Experiment

A photograph of the setup used for our experiments is shown in Fig. 3. The krypton (Kr) laser at the far left has an output of 400 mw at 647.1 nm. Following the laser are lenses and a cylindrical mirror (at the far right) which transforms the circular laser beam into a uniform intensity sheet beam 15-cm wide by 60-μm high at the position where the $LiNbO_3$ or BGO SAW delay lines are mounted. Following the SAW lines, a cylindrical lens and parabolic mirror are used to focus the light onto a PIN photodiode having less than 1-ns response time. The photodiode signal is then amplified by wide-band amplifiers.

Fig. 4 shows a closeup of a $LiNbO_3$ and a BGO line placed side-by-side in the "two-crystal" correlator configuration (the BGO is

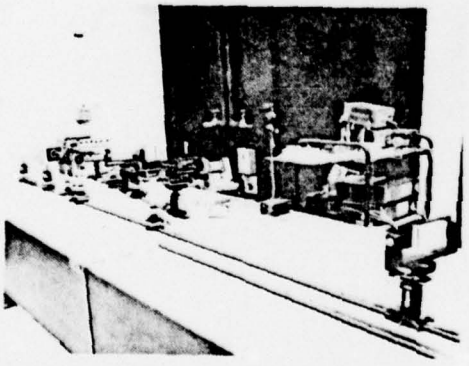

Fig. 3. Experimental Setup for Real-Time Acousto-Optic Signal Processing.

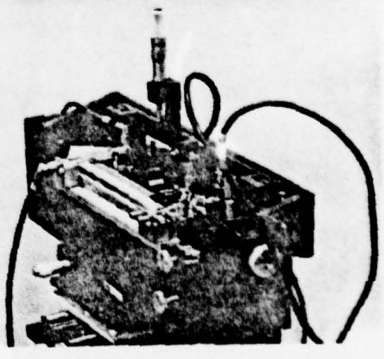

Fig. 4. $LiNbO_3$ and BGO Delay Lines Used for Acousto-Optic Signal Processing.

the darker crystal). The dimensions of each crystal were 15 x 1 x 1 cm. The $LiNbO_3$ used was Y-cut, Z-propagating, and the BGO used was 001-cut, 110-propagating. In both crystals, the SAW propagation direction was in the long dimension. To insure maximum acousto-optic coupling, it was necessary to obtain extremely good surface figure and polish on the crystals. The top surfaces of the crystals were polished to a figure of about one wave ($\lambda \sim 0.55$ μm) over the entire 15 x 1 cm area, with no visible defect marks under 100X magnification. Both sides of the crystals upon which the laser light impinges were polished so as to have no more than 0.5° deviation from perpendicularity with the top surface. Each of the two long edges were made as chip-free as possible. Chip length was no more than 25 μm, and the total length occupied by chips was less than 2% of the 15-cm length. The impinging Kr laser light beam was perpendicular to and filled the long dimension of the lines. The actual laser light intensity through the region of SAW propagation was approximately 10 mW.

Interdigitated finger transducers were used to convert the rf signals into SAW's. To achieve a large interaction bandwidth, a series of four transducers was used for this conversion. The center frequencies of these transducers in $LiNbO_3$ were 250, 355, 475, and 612 MHz. The center frequencies in BGO were lower by a factor equal to the ratio of the respective SAW velocities in $LiNbO_3$ and BGO (~2.075). The transducers were tilted slightly with respect to each other according to a scheme by Tsai.[4] In this manner, the Bragg condition was satisfied simultaneously for all four center frequencies, thereby permitting a large instantaneous bandwidth. In addition, the transducers were translated with respect to each other in the direction of wave propagation to provide proper phase matching at the crossover frequencies.

Each device was operated initially as a convolver. For BGO and $LiNbO_3$, input bandwidths of 140 and 250 MHz, respectively, were obtained. For both devices, the full design bandwidth was not achieved, because of very high insertion losses for the highest frequency transducer in each device and because of the response roll-off of the photodetector and amplifiers above 800 MHz. Interaction lengths of 65 and 40 μs, respectively, were obtained for the BGO and $LiNbO_3$. These lengths corresponded exactly to the physical interaction lengths available in each device. The time-bandwidth product of these devices used as convolvers, obtained by multiplying the bandwidth with the interaction time, was 9100 for the BGO device and 10,000 for the $LiNbO_3$ device.

The acousto-optic correlator shown in Fig. 4 has been used successfully to correlate several waveforms of interest in radar applications. Fig. 5A shows the output obtained by correlating two monofrequency square-wave pulses for a low-frequency correlator ($LiNbO_3$

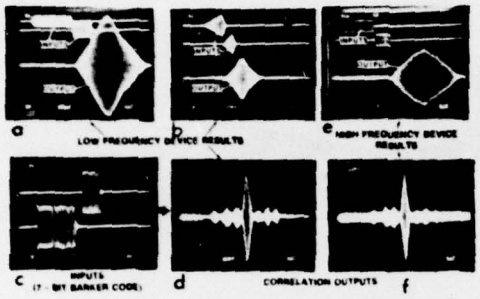

Fig. 5. Real-Time Correlation Output Obtained with Two Rectangular Waveforms (a) and (e) and with Seven-Bit Barker Code (d) and (f).

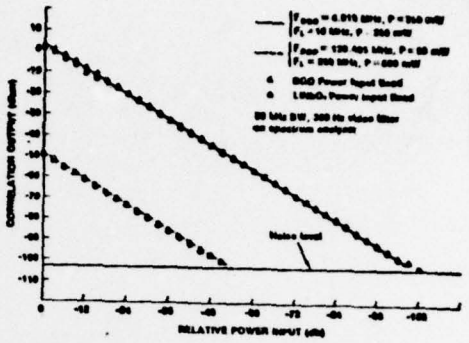

Fig. 6. Correlation Output versus Input Power, Demonstrating Linear Dynamic Range of Acousto-Optic Correlator.

at 10 MHz and BGO at ~5 MHz), and Fig. 5E shows the corresponding result for the high-frequency correlator. The output pulsewidth is about four times longer than the short ($LiNbO_3$) input pulse, as expected. Fig. 5D and 5F show the results, in the low- and high-frequency devices respectively, of correlating the seven-bit Barker code[5] shown in Fig. 5C. There is a strong central peak with three sidelobes on either side, as expected. The peak-to-sidelobe ratio appears to be just slightly greater than the theoretically expected 2.7:1 ratio.

The results of measurements of the dynamic range of both the low- and high-frequency acousto-optic correlators are shown in Fig. 6. Because of much lower transducer insertion loss at low frequencies, the low-frequency correlator exhibited a greater dynamic range. Extrapolating to a reference 1-MHz bandwidth, a dynamic range of about 84 dB is obtained. The output is linear over this entire range for variations of either the BGO or the $LiNbO_3$ input.

C. Applications

1) Signal-to-Noise Ratio Enhancement

One of the major functions of an acousto-optic correlator in radar applications would be to extract signals submerged in noise. It can be shown[6] that the most effective means of extracting a signal from noise is by using a matched filter. A correlator is by definition an adaptive matched filter, i.e., its response is the equivalent to a matched-filter response for any waveform corresponding to the reference waveform. The time-bandwidth product of the filter is a

direct measure of the signal-to-noise (S/N) enhancement. Hence, the relatively large time-bandwidth product, as well as the range of the instantaneous bandwidth, of the real-time acousto-optic processors described above make them very attractive candidates for advanced radar processing. Examples of the ability of the acousto-optic correlator to extract signals buried in noise are shown in Figs. 7 to 10. In Fig. 7 the output of the correlator is shown both for a noise-free and a noisy (S/N = -10 dB) monotone input signal. Figure 8 is a quantitative plot of output S/N versus input S/N for monotone inputs.

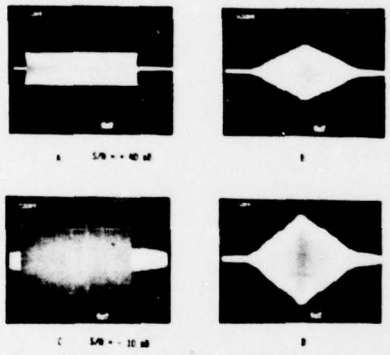

Fig. 7. Convolution Output with Noisefree Input (B and A) and with Noise-Degraded Input (D and C).

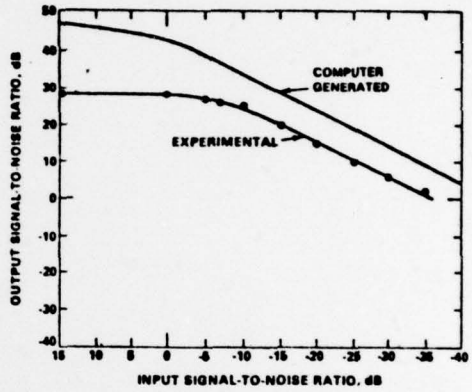

Fig. 8. Signal-to-Noise Enhancement as Obtained with a Digital Computer, Compared with Acousto-Optic Experimental Results.

The computer-generated result is based on an equivalent time-bandwidth product of 30,000, whereas the particular acousto-optic device had a time-bandwidth product of 7,500. Fig. 9 illustrates qualitatively the S/N enhancement for 100-MHz bandwidth, 20-μs wide, linear FM chirps. Fig. 10 illustrates quantitatively the enhancement for these broadband signals. In all cases, a S/N enhancement on the order of 30 dB is possible.

2) Fourier Transformation

The ability to perform real-time Fourier analysis of rf signals is important in both communication and signal-warfare systems. Fourier transforms have been performed acousto-optically using the "chirp transform" method[7], and a signal-processing architecture for performing discrete Fourier transforms acousto-optically has been devised.

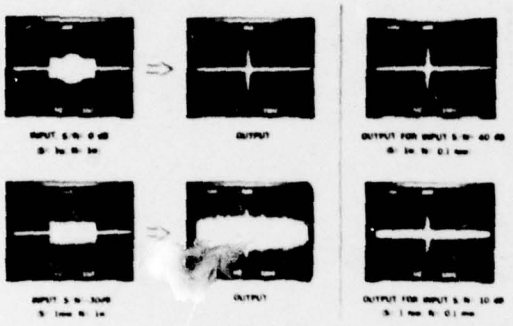

Fig. 9. Signal-to-Noise Enhancement with 100-MHz Bandwidth Linear FM Chirp Signals.

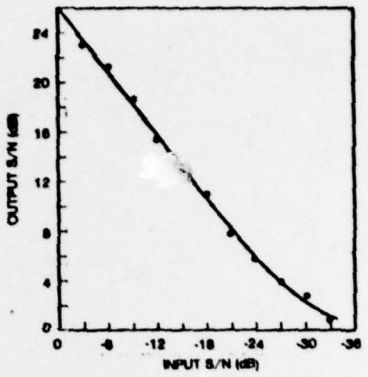

Fig. 10. Output Signal-to-Noise versus Input Signal-to-Noise for 100-MHz Bandwidth Signals.

a. Real-Time Chirp Transform

The Fourier Transform of a function x(t) is defined as

$$X(f) = \int_{-\infty}^{\infty} e^{-i2\pi ft}\, x(t)dt \ . \qquad (6)$$

If the substitution $-2ft = (f - t)^2 - f^2 - t^2$ is made in eq. (6) and the terms rearranged, the following is obtained:

$$X(f) = e^{-i\pi f^2} \int_{-\infty}^{\infty} [e^{-i\pi t^2}\, x(t)][e^{i\pi(f-t)^2}]dt \ , \qquad (7)$$

where the first bracketed term in the integral is identified as a premultiplication of the function x(t) by a chirp. This premultiplied term is then correlated with a chirp. Finally, the correlation result is postmultiplied by a chirp. This entire sequence is referred to as the "chirp transform" implementation of the Fourier transform.

The acousto-optic devices described in section IIB were used to perform the correlation portion of this transform, and the required chirps were obtained from an impulse-excited, reflective-array-compressor SAW delay line. The results of this implementation are summarized in Figs. 11 to 14. The measured bandwidth of the transformer was about 80 MHz, as illustrated in Fig. 11 where the transformed output of a pulse containing three discrete frequencies is

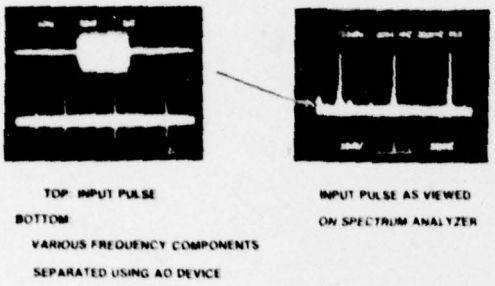

Fig. 11. Fourier Transform (lower trace) of Gated Signal (top trace) Containing Discrete Frequencies 18, 54, and 90 MHz.

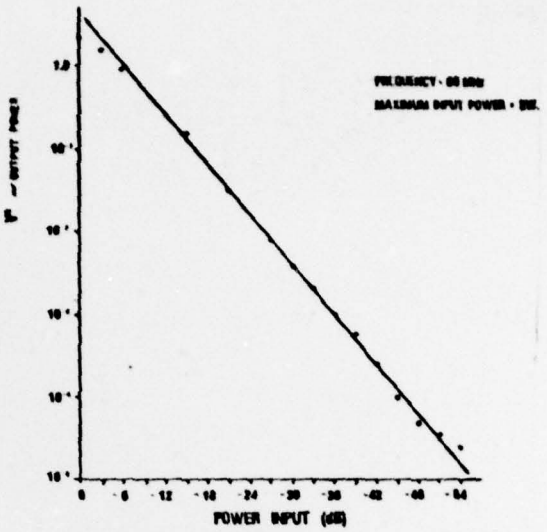

Fig. 12. Dynamic Range of the Acousto-Optic Fourier Transform Output.

shown. The dynamic range for the cw-gated signal exceeds 50 dB and is shown in Fig. 12. The structure of the sidelobes is strongly dependent on the spatial distribution of the light intensity of the incident laser beam. If a uniform intensity distribution is used, then a (sin x)/x sidelobe pattern results (Fig. 13). When illuminated with a Gaussian profile, the sidelobes were suppressed to about 27 dB below the main peak, as is shown in Fig. 14. The sidelobe amplitude is compared with a second, nearby, signal which is 25 dB down from the main signal.

These results are generally in accord with the best reported results obtained by using a pure SAW filter approach to achieve chirp transformation.[8] The advantages of the acousto-optic approach, however, are twofold: i) the ease in applying weighting functions for sidelobe suppression, and ii) the capability of arbitrarily varying the chirp rate, which aids in locating signals.

b. Discrete Fourier Transform

An alternative to the chirp-transform architecture has been proposed which is especially useful when performing the discrete Fourier transform (DFT). The DFT is defined as

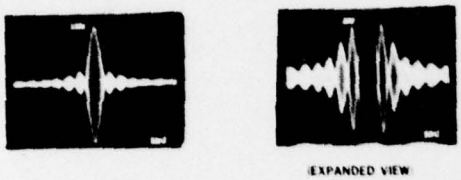

Fig. 13. Sidelobe pattern ($\frac{\sin x}{x}$) of the Acousto-Optic Fourier Transform Obtained Using a Uniform-Intensity Laser-Beam Profile.

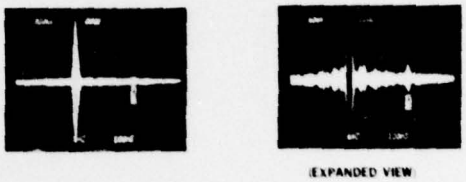

Fig. 14. Suppressed Sidelobe Pattern of the Acousto-Optic Fourier Transform Obtained Using a Gaussian Intensity, Laser Beam Profile; Pattern Compared with Higher Frequency Signal (arrow) at -25 dB.

$$X_k = \sum_{n=0}^{N-1} x_n \, e^{-i2\pi nk/N} \, . \tag{8}$$

If the substitution

$$nk = \frac{1}{4}\{(k+n)^2 - (k-n)^2\} \tag{9}$$

is made into eq. (8), the following results:

$$X_k = \sum_{n=0}^{N-1} x_n \, e^{\frac{-i\pi(k+n)^2}{2N}} \, e^{\frac{i\pi(k-n)^2}{2N}} \, . \tag{10}$$

The exponential factors in eq. (10) can be interpreted as two (chirp) waves propagating in opposite directions relative to the function to be transformed. This transform architecture is referred to as the triple-product convolver[9] and can easily be realized using acousto-optic techniques. This architecture is illustrated in Fig. 15. The large sheet beam used in the previous implementations of the acousto-optic convolver is now replaced by a series of very narrow laser beams

where the amplitude of each laser beam is modulated (e.g., by an electro-optic crystal) in accord with the input digital data stream which is to be transformed. This structure is being constructed at the Harry Diamond Laboratories.

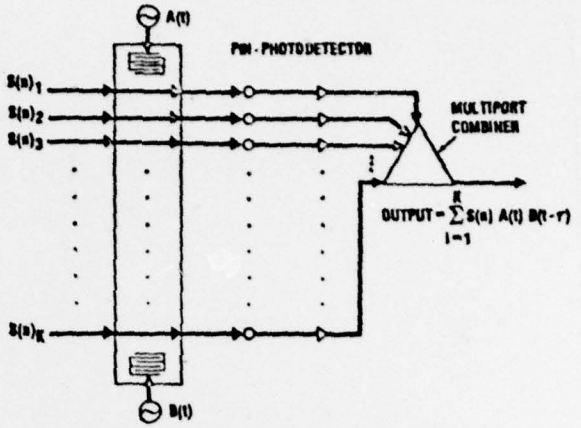

Fig. 15. Architecture for an Acousto-Optic Triple-Product Convolver.

III. Acousto-Optic Memory Correlator

A. Acousto-Photorefractive Effect

A new photorefractive effect has been discovered whereby an index-of-refraction change (δn) in $LiNbO_3$ results from the interaction of high-intensity, short-duration laser pulses with propagating surface acoustic waves. This acousto-photorefractive effect can be used to implement an acousto-optic memory correlator. This effect is phenomenologically similar to a nonlinear "two-photon" photorefractive effect reported previously,[10] but is not a simple extension of that effect. In the present experiment, an SAW pattern was stored as δn. The δn was found to be proportional to the rf amplitude, and increased sublinearly (0.7 power) with the number of laser pulses and as the 1.3 power of the incident laser energy density. The decay time varied from a few hours, when only green illumination (530 nm) was used, to several weeks, when combined green and infrared (IR) illumination (1060 nm) were used. The δn can be erased by exposure to ultraviolet radiation or by annealing at 250°C.

An acousto-optic memory correlator has been constructed wherein both the stored δn and the δn produced by a "live" propagating acoustic wave simultaneously modulate a low-power cw laser beam. The resultant detected signal is proportional to the correlation integral. The memory correlator operated at a center frequency of 10 MHz with a 1-MHz bandwidth. A large variety of complex signals, such as chirps and Barker codes, was stored and subsequently correlated. The stored signal strength was about 30 dB below that of the original live signal, and successful correlation with a live signal was achieved several weeks after storage.

A sketch of the setup used for our experiments is shown in Fig. 16. During the writing (storage) phase, illustrated at the left of the figure, a neodymium: yttrium aluminum garnet (Nd:YAG) laser was used in which the output was a single-mode (TEM_{oo}) Gaussian pulse

having a 12-ns pulsewidth and an energy of 100 mJ/ pulse. The 1060-nm IR output was converted to green (530 nm) by using either a CD*A temperature-tuned or a KDP angle-tuned doubler. By means of appropriate lenses, the resultant light was converted into a sheet beam about 1 cm wide and 250 μm thick. This sheet beam was then focused along the top edge of the side of the $LiNbO_3$ crystal, so that it passed through the region of SAW propagation. Since many pulses were often used for storing a signal, the launching of the acoustic waves was synchronized with the writing (Nd:YAG) laser pulse to within 3 ns of uncertainty. The synchronization was done to assure that the acoustic wave was in the same position during each laser pulse. The light beams used for both writing and reading were incident along the x-axis, perpendicular to the z-direction (optical c-axis) of acoustic propagation.

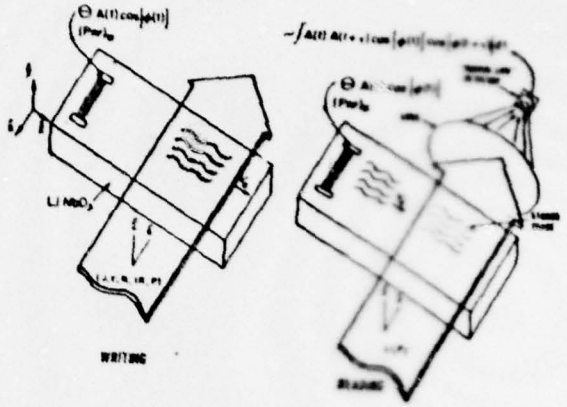

Fig. 16. Acousto-Optic Correlator in Both Writing (left) and Reading (right) Modes.

The reading phase, illustrated at the right of Fig. 16, was accomplished with a 10-mW cw He-Ne laser. Since the index-of-refraction pattern stored by the acousto-photorefractive effect was only a small ac component riding on top of a much larger ($\sim 10^3$) dc index change, the ac signal could not be measured by the means used conventionally for observing δn. Two methods were used for observing these changes. The presence of an ac index-of-refraction pattern could be verified qualitatively by observing the diffraction of light transmitted through this newly formed diffraction grating. Quantitative information was obtained by propagating a live acoustic wave in the crystal during illumination with the low-intensity cw reading laser. Both the stored and live signals modulated the light beam via the Bragg acousto-optic interaction. The doubly modulated light was focused onto a "square-law" detector diode the output of which is proportional to the correlation of the two acoustic signals.[3]

In the experiments described here, the δn was obtained in plates of Y-cut Z-propagating single-crystal $LiNbO_3$ which had been fabricated into SAW delay lines by the deposition of interdigitated-finger transducers at each end. The spacing between transducers was 7 cm, corresponding to a delay of about 20 μs. The acoustic aperture of the

transducers was 1.5 cm, and their center frequency was 10 MHz with a 1-MHz bandwidth.

The variation of correlation output power $(\sim\delta n^2)^{(2)}$ was measured as a function of number of laser pulses (N), incident laser energy density (J), and rf input power during storage (P). These results have been summarized into the graph presented as Fig. 17. The axes are the number of laser pulses (N) and laser energy density (J/cm^2) per pulse, with lines of constant insertion loss plotted in the figure. Insertion loss is defined here with respect to the known output obtained from the "live" convolution of two 10-mW signals in an acousto-optic convolver. It should be observed from Fig. 17 that for a single laser storage pulse of 10^3 mJ/cm^2, which is still below the damage threshold for $LiNbO_3$, the insertion loss is ~30 dB. Fig. 18

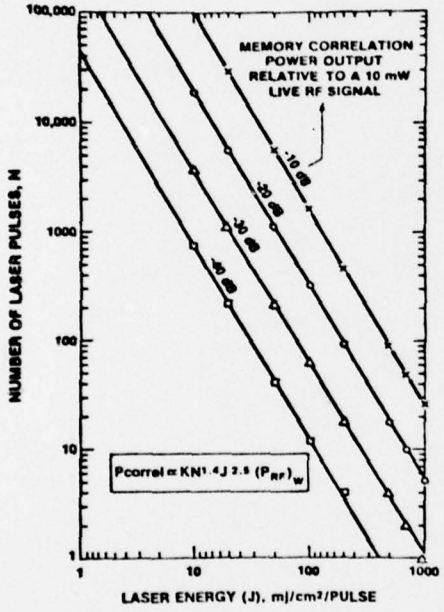

Fig. 17. Curves of Constant Output Power from Memory Correlator as Function of Number of Laser Pulses and of Laser Energy Density.

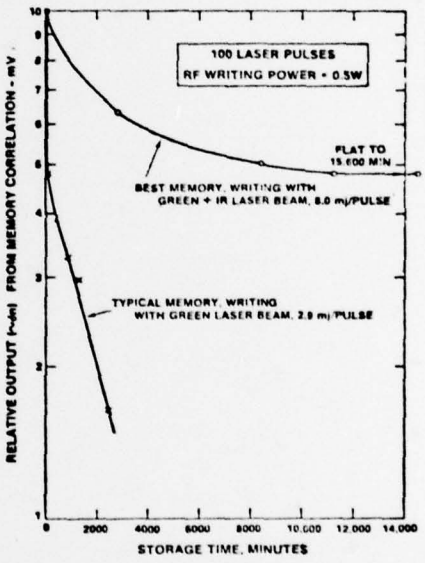

Fig. 18. Relative Correlator Output Power versus Storage Time for Two Cases, Green Writing Beam Alone and Combined Green and IR Writing Beam.

shows a plot of the decay of δn at room temperature as a function of time after storage for two cases: (1) green illumination only and (2) green with IR. The two cases show different time constants, the time constants for the second case being several orders of magnitude

larger than those for the first. We believe that the relatively flat regime obtained with the second case is probably the long-term natural decay time for charge in a relatively pure dielectric.[11]

The physical basis of the acousto-photorefractive effect appears to be the movement of charge which results in a change in the local index of refraction via the electro-optic effect. Because of the magnitude of the effect, we speculate that the electric field accompanying the acoustic wave in the piezoelectric materials, rather than density changes alone, may be responsible for this movement of charge.

B. Applications

The acousto-photorefractive effect may be used to construct an acousto-optic memory correlator that is generically similar to an acousto-electric memory correlator reported previously.[12] Successful correlation of live signals consisting of relatively complex waveforms has been accomplished with waveforms that were stored for as long as several weeks. These data are summarized in Figs. 19 and 20.

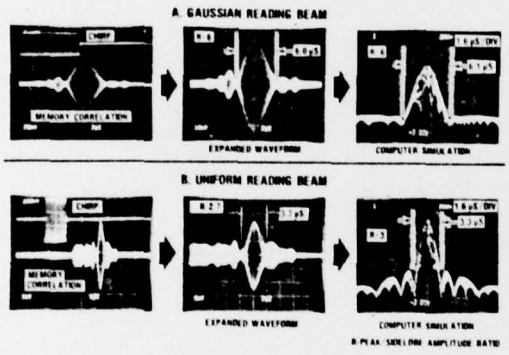

Fig. 19. Output Waveforms of Memory Correlator and Comparison with Computer Simulation for Linear FM Chirp by Using Both Gaussian and Uniform Reading Beams.

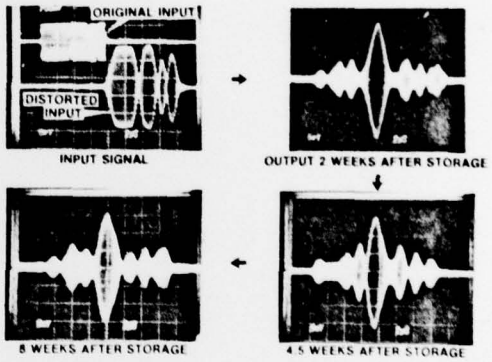

Fig. 20. Changes with Time of Output Waveforms of Memory Correlator for Seven-Bit Barker Code.

Fig. 19 illustrates the output obtained by correlating a live 10 MHz, 10-μs wide rectangular pulse having a linear FM chirp of about 1 MHz against a similar previously stored signal. In Fig. 19A, the reading beam used had a Gaussian intensity distribution across the length of the stored image; Fig. 19B pictures were obtained for a uniform beam intensity. Comparison of the expanded output pulses with the computer simulations (shown at the right of Fig. 19) for both types of beam distribution demonstrates good agreement for both the null-to-null spacings and the peak-to-sidelobe ratio (R).

Fig. 20 indicates the observed changes of the output of the seven-bit Barker code correlation as a function of time. The slow

degradation of the stored pattern manifested itself in a distortion of the sidelobes; however, the main correlation peak remained relatively unchanged.

IV. Conclusions

Two new types of acousto-optic signal processors have been demonstrated. The first is a real-time correlator having a large time-bandwidth product (~3,000). This device has been used to perform Fourier transformation (>50 dB dynamic range), as well as signal-to-noise enhancement (>30 dB). The second type of processor is a memory correlator in which signals may be stored for long periods of time, and in which live signals may subsequently be correlated with the stored signals. The feasibility of storing and correlating with complex, phase-coded waveforms for up to two months has been demonstrated. Both of these signal processors should find many applications in radar, communications, and signal-warfare systems.

References

1. N. J. Berg, B. J. Udelson, and J. N. Lee, Appl. Phys. Lett. 31 (1977), 555.
2. R. Adler, IEEE Spectrum, 4 (1967), 42.
3. N. J. Berg, B. J. Udelson, J. N. Lee, and E. Katzen, Appl. Phys. Lett. 32 (1978), 85.
4. T. S. Tsai, L. T. Nguyen, S. K. Yau, and M. A. Alhaider, Appl. Phys. Lett. 26 (1975), 140.
5. C. E. Cook and M. Bernfeld, Radar Signals, Academic Press, New York (1967), 245-247.
6. M. I. Skolnik, Introduction to Radar Systems, McGraw-Hill, New York (1962), Ch. 9.
7. L. R. Rabiner, R. W. Schafer, and C. M. Rader, IEEE Transactions on Audio and Electroacoustics AU17, No. 2 (1969), 86.
8. H. M. Gerard, P. S. Yao and O. W. Otto, Proc. IEEE Ultrasonics Symp. (1977), 77CH1264-1SU, p. 947.
9. J. M. Speiser and H. J. Whitehouse, Naval Ocean System Center, San Diego, CA, NUCTN 1355R (1974).
10. D. von Linde, A. M. Glass, and K. F. Rodgers, Appl. Phys. Lett. 25 (1974), 155.
11. J. P. Huignard, F. Micheron, and E. Spitz, Optical Systems for Photosensitive Materials for Information Storage, North-Holland, Amsterdam (1976), Ch. 16.
12. A. Bers and J. H. Cafarella, Appl. Phys. Lett. 25 (1974), 133.